Speed Profile Generation Strategy for Efficient Merging of Automated Vehicles on Roundabouts with Realistic Traffic

Juan Felipe Medina-Lee, Jorge Godoy, Antonio Artuñedo and Jorge Villagra

***Abstract*—The capabilities of automated vehicles have increased over the last years, and different driving strategies have shown promising results on a variety of scenarios. However, there are still many challenges to be solved, and handling crowded roundabouts is one of them. This kind of scenario requires both safe and efficient maneuvers from the autonomous driving systems in order to maintain a proper traffic flow. This work presents a strategy to generate different speed profiles for a set of path candidates in order to obtain a merging maneuver according to current traffic scene. The proposed mechanism relies on the use of fictitious accelerations generated by leader and lag vehicles, incorporating by design comfort and safety bounds. The autonomous driving system proposed in this work was tested on realistic driving scenarios collected from public datasets and its performance was compared to human drivers on the same scenarios. The results showed in a variety of situations that the automated vehicle was capable of merging into roundabouts with tight merging gaps while maintaining both comfort and safety constraints.**

***Index Terms*—Autonomous driving, motion planning, trajectory generation, speed profile, roundabouts, merging algorithm.**

I. Introduction

AUTONOMOUS driving systems (ADS) have shown great improvement over the recent years. However, there are still some challenges to be resolved before Autonomous Vehicles (AV) can properly drive on highly dynamic scenarios like urban roundabouts [1]. Even though the use of these road layouts has significantly increased over the years, the roundabouts crossing problem for AV has received little attention in the literature [2]. A specific challenge to be addressed in the design of roundabout-oriented ADS is their overly cautious behavior, that in the interests of ensuring safety, can produce unhuman-like behavior. Such conservative behaviors can degrade the driving quality and may jeopardize safety when the ADS decisions are not expected by other road participants [3].

The state-of-the art in cooperative speed planning for Connected and Automated Vehicles (CAV) often rely on optimization and control schemes [4] [5] whose goal is to determine a speed profile for each involved vehicle. Their deployment is in different degrees of progress, but they were mainly designed to applications where automation levels are not necessarily too high. If stand-alone highly automated vehicles are targeted, speed planning requires a higher flexibility and closer connection with path and maneuver planners. This is particularly true in complex urban scenarios, such as roundabouts, for which some previous works exist. The authors in [6] propose a two-stage optimization model to handle traffic on roundabouts for fully connected automated vehicles equipped with Vehicle-to-Infrastructure (V2I) and Vehicle-to-Vehicle (V2V) technologies. The first stage optimizes the vehicle arrival time at the roundabout, while the second stage optimizes the vehicle trajectories by minimizing the acceleration fluctuation. In [7] it is proposed a collaborative strategy using V2V for handling traffic on intersections and roundabouts, where the speed of the vehicles is reduced or increased according to the expected time to reach the end of the intersection. In [8] the vehicles merging into the roundabout are coordinated using a Roundabout Coordination Unit (RCU) that determines the acceleration of automated vehicles for a smooth merging and to avoid collisions. In the case of [9], the authors propose a decision making algorithm considering personalized driving behaviors while using Model Predictive Control (MPC). These vehicle-to-everything (V2X) approaches show promising results, but it will not be easy to see them deployed in a near future, as not all vehicles may have the required connectivity and perception technologies.

Different path planning primitives have been tested in roundabouts scenarios, e.g. Bézier [10], splines [11] or clothoids [12]. However, these works did not consider other traffic agents on the scene. To cope with this limitation, some studies take into consideration the evolution of traffic using their on-board perception system. In [13] the authors propose a tactical behavior planner to navigate on roundabouts, which selects the most appropriate trajectory according to a multi-objective function. In the case of [14], the ADS uses a hybrid trajectory planning combining Bézier curves for the path generation and MPC for the speed control of the Ego-Vehicle (EV). The authors in [1] propose a trajectory planner using support vector machine to identify the collision-free space and to simultaneously generate the path and the speed profile for the EV. All these contributions were tested on controlled and limited traffic scenes, where only one Other Vehicle (OV) was present in the roundabout at the moment of the merging maneuver.

In [2], the authors propose a strategy for an ADS to cross roundabouts in a safely manner; they use virtual instances of the vehicles in the roundabout and validate the behavior

The authors are with the Centro de Automática y Robótica, CSIC-Universidad Politécnica de Madrid, 28500 Arganda del Rey, Madrid, Spain. (email: juan.medina@csic.es; jorge.godoy@csic.es; antonio.artunedo@csic.es; jorge.villagra@csic.es).

of their system using realistic scenes from data sets. For the speed profile generation proposed in this work they set maximum nominal speed when there is no leader vehicle on the roundabout, or set the same speed as the leader vehicle in case it exists. The planner proposed in [13] generates trajectory candidates with speed profiles based on Bézier curves with different final speeds, which are created according to comfort requirements, and then selects a trajectory that maximizes a behavior selection function. The decision making algorithm proposed in [15] uses a game-theoretic model that represents the interactions between the EV and OVs, and adapts them depending on an estimated driver type; the speed of the EV is generated by selecting an action from a discrete action set, which allows to maintain the current speed, brake at a constant deceleration or fully accelerate. These works can work under different traffic conditions, but the speed profile generation for the EV either is too simplistic or it does not consider the state of the OVs to properly adapt to the current traffic situation.

In the light of the above, the literature on decision making for on-road AVs is very sparse in terms of works dealing with the efficient on-board management of roundabouts with traffic. Indeed, although partial contributions exist, there is a need to simultaneously cope with the following four challenges:

- avoid overcautious behaviors when entering and leaving the roundabout;
- test not only on specific and limited traffic, but on generic layouts and with different replicable traffic patterns;
- operate irrespective of whether there is an external coordination unit to control connected vehicles;
- avoid the generation of speed profiles that are too simplistic or do not take into account the traffic status in the roundabout, leading to unpredictable maneuvers.

In this work, a novel strategy is proposed dealing with these challenges. A set of possible trajectories is generated based on both the geometry of the road and the status of the OVs, obtaining thus a safe, yet efficient maneuver when facing a roundabout. The overcautious behavior of the resulting trajectories is modulated with virtual accelerations induced by the lead and lag vehicles. The generation of multiple candidates with different acceleration limits allows the ADS to explore a large diversity of trajectories and select the best of them according to a merit function, enhancing the performance of the very few similar existing approaches. Note that this strategy, designed to deal with the complexity of roundabouts, is fully operational in other driving scenarios -as shown in [16]- and could be compatible with works like [17] to handle platoons merging and splitting maneuvers.

In order to evaluate the performance of the trajectory generation algorithm, realistic traffic scenes from the `openDD` dataset [18] were recreated on a simulation environment. The main contributions of this work with respect to the existing motion planning literature can be summarized in the four following points:

- A speed profile generation strategy that takes into account the evolution of obstacles present in the driving scene and is seamlessly integrated with a path planner to dynamically adjust the acceleration along the path. The resulting algorithm is able to explore, provoke and maintain safety gaps with potential lag or leader vehicles, while meeting comfort constraints and achieving a high degree of traffic efficiency.
- Validation of the proposed strategy on naturalistic and replicable roundabouts scenes, obtained from the `openDD` dataset and implemented in a software-in-the loop simulation framework.
- Performance comparison of the proposed trajectory generator on realistic and dense traffic scenarios with respect to different human drivers and to another state-of-the-art technique.
- Evaluation of the trajectory generation robustness when facing speed variations of the involved vehicles in naturalistic traffic scenes.

The outline of the paper is as follows: Section II presents an overview of the ADS architecture and different aspects to take into consideration when facing a roundabout. Section III describes the speed profile generation strategy to handle a roundabout. The experimental results are shown in Section IV. Finally, Section V presents the concluding remarks.

II. Autonomous driving framework

A. ADS architecture

As can be seen in Fig. 1, the ADS proposed in this work is divided in different modules with specific tasks in the driving process. The global router receives the destination point and calculates the complete route from the current position of the EV to the destination using a digital map on a *lanelet2* format [19]. The perception module determines the status of traffic agents present on the scene. In this work it is assumed that the OVs pose and dimensions are known; the reader may find in [20] an implementation of the perception module. Another function of this module is to compute the motion predictions of the vehicles present in the scene, described in detail in [21]. The maneuver planner module identifies the reachable navigation corridors based on the EV position and selects the most appropriate one considering the global route and the state of other traffic agents. The Trajectory Generator (TG) module creates a valid set of trajectories (Γ) and selects the best of them (Γ_b) using a merit function that combines four Decision Variables (DV): longitudinal comfort, lateral comfort, safety and utility according to a set of weights ω which allows to customize the driving style by prioritizing one or more DVs over the others. In order to obtain Γ, a path set $\mathcal{P}$ is generated using quintic Bézier curves, and, for each path candidate $\rho \in \mathcal{P}$, different speed profiles are computed to meet both comfort and safety constraints. A complete description of the merit function and the trajectory generation process is presented in [16]. The main focus of this paper is to propose a strategy to generate valid speed profiles for each path to perform an efficient roundabout merging, as described in section III. Finally, the control module calculates the throttle, braking and steering wheel commands to track Γ_b.

B. Possible driving scenarios when facing a roundabout

When the EV is heading into a roundabout it has to decide whether (i) it merges before an OV already driving on the

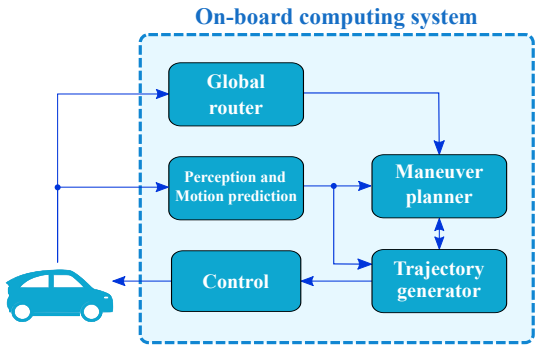

Fig. 1. Block diagram of the ADS architecture.

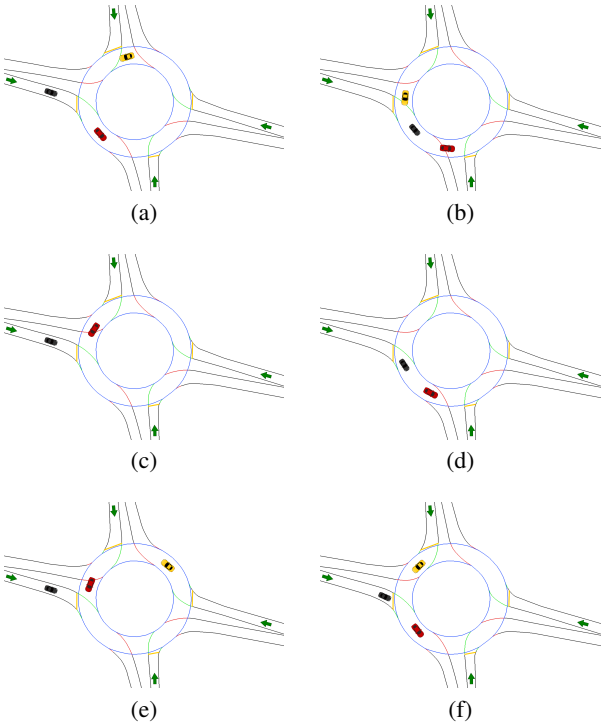

Fig. 2. Possible merging scenarios on a roundabout. (a-b) Merging before another vehicle. (c-d) Merging after another vehicle. (e-f) Stopping on yield line.

roundabout, (ii) it slows down to merge into the roundabout after an OV or (iii) it stops on the yield line. These scenarios are presented on Fig. 2.

Fig. 2a shows the initial moment of a driving scenario where the EV (black) is heading into a roundabout with a leader vehicle OV_{lead} (red) and a lag vehicle OV_{lag} (yellow) driving on the roundabout-ring; in this scenario, the EV is able to merge before OV_{lag}, as shown on Fig. 2b. For this type of scenario, OV_{lead} may not exist. Fig. 2c shows the second possible scenario, where there is a vehicle on the roundabout and it is not possible to merge before it passes the intersection point. In that case, the EV must reduce its speed so it can merge after the OV without stopping on the yield line, as shown on the Fig. 2d. In the last scenario, there is dense traffic on the roundabout (see Fig. 2e) and the EV has to stop on the yield line to wait for a large enough gap to merge on the roundabout (Fig. 2f).

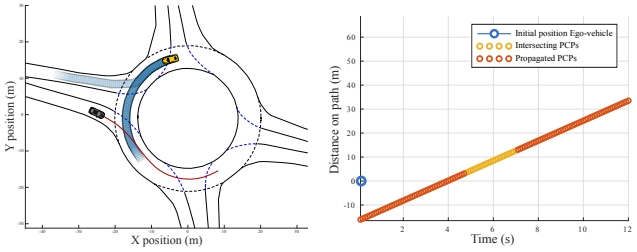

Fig. 3. PCPs created for an obstacle driving inside a roundabout during a merging maneuver. (a) Obstacle predicted positions. (b) Possible collision points.

C. Possible Collision Points

In order to compute the merging speed profile for each $\rho \in \mathcal{P}$, the predictions of the OVs are projected into ρ using a spatio-temporal representation. These projections are computed by finding intersections between the polygon occupied by the EV when following ρ and the predicted positions of the OVs. Each time a prediction of an OV intersects with the ρ, a single point is created. This projections will be referred to as Possible Collision Points (PCP). The PCPs also contain information about the ID and the speed of the OV (see [22] for more details). Fig. 3a shows the predictions for a time interval $t \in [0, 7s]$ of an OV (yellow vehicle) driving inside a roundabout and a path candidate $\rho \in \mathcal{P}$ (red line). It can be observed that some of the predicted positions for the OV intersect with ρ. The resulting PCPs for this scenario are displayed on Fig. 3b. The yellow circles represent the projected positions on ρ of the intersecting predictions, which start at $t = 4.8s$; the orange circles are inferred positions of the OV along ρ computed from the yellow points. The initial position of the EV on ρ is $x_{ego} = 0\,m$, hence, an OV is considered as an OV_{lag} if the position of its PCP at $t = 0s$ is lower than $0m$. In the driving scenario of Fig. 3, the yellow OV inside the roundabout is considered an OV_{lag} since the position of its PCP at $t = 0s$ is $PCP_{t=0} = -16.5m$.

III. Speed Profile Generation

For each path candidate $\rho \in \mathcal{P}$, a fixed number N_{sp} of speed profiles are generated, each of them with different acceleration limits to increase the reaching possibilities of the trajectory set. The first step is to compute an obstacle-free speed profile Λ that takes into account the path geometry as well as lateral and longitudinal comfort acceleration constraints. Then, using Λ as the highest limit, a traffic-based speed profile $\mathbf{V}_{ego}$ is built considering the obstacles present on the scene. The process of the speed profile generation when there are only leader vehicles on the scene is described on [16]. In this work, a complimentary strategy is proposed for generating both Λ and $\mathbf{V}_{ego}$ on crowded roundabouts.

Fig. 4 shows a data flow diagram of the algorithm that generates the speed profile for each ρ when a roundabout scenario is found by the EV. If there is an OV_{lag} driving on the roundabout, $\mathbf{V}_{ego}$ will attempt to merge into the roundabout before OV_{lag} gets into the intersection point. If that maneuver is not feasible because safe distances with respect to OV_{lag}

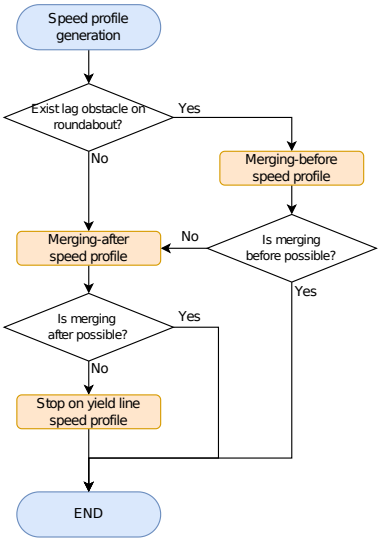

Fig. 4. Speed profile generation algorithm for roundabouts

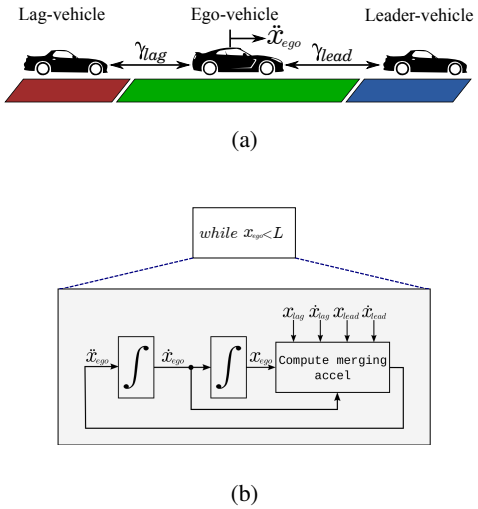

Fig. 5. Merging before another vehicle model. (a) Influences γ_{lag} and γ_{lead} from the OV. (b) Iterative process of speed profile generation.

and OV_{lead} (if present) cannot be guaranteed, a new $\mathbf{V}_{ego}$ is created so that the EV merges after OV_{lag}. Finally, if it is not possible to merge into the roundabout without stopping, $\mathbf{V}_{ego}$ will lead the EV to stop on the yield line. If there is an OV also heading into the roundabout between the EV and the yield line, then $\mathbf{V}_{ego}$ will use the inter-distance strategy proposed in [16] instead of the algorithm of Fig. 4. The location of the EV on the digital map is used to improve the consistency of the maneuvers over time i.e., in case the decision was to merge before an OV_{lag}, this decision cannot be changed once the EV has entered the roundabout-entrance zone (green lanes of Fig. 2) for safety reasons. Or when the EV is traveling on the roundabout-ring, the speed profile is generated taking into account the higher priority of that road over incoming vehicles into the roundabout.

A. Merging before another vehicle

The speed profile to merge before OV_{lag} is generated using the following approach: the OV_{lag} has a push-forward influence γ_{lag} on the EV acceleration, while the OV_{lead} has a push-back influence γ_{lead} on the EV. The acceleration of the EV ($\ddot{x}_{ego}$) is computed by combining those influences, considering the gap distance and the speed difference with respect to both OV_{lag} and OV_{lead}. This model is illustrated on Fig. 5a. Once $\ddot{x}_{ego}$ is calculated, it is integrated to obtain a new value of $\dot{x}_{ego}$ which is appended to $\mathbf{V}_{ego}$. Finally, $\dot{x}_{ego}$ is integrated to update the position of the EV on the path. This process is repeated as long as x_{ego} is lower than the length L of ρ, as depicted on Fig. 5b. The positions and speeds of the leader and lag vehicles ($x_{lag}, \dot{x}_{lag}, x_{lead}, \dot{x}_{lead}$) are updated using the information of the PCPs (described in II-C).

The computation of γ_{lag} takes into account the speed difference between the EV and the OV_{lag} as follows:

$$\gamma_{lag} = \begin{cases} \gamma_{max}, & \text{if } \dot{x}_{ego} < \dot{x}_{lag}, \\ \gamma_{mlag}, & \text{if } \dot{x}_{lag} \leqslant \dot{x}_{ego} < \dot{x}_{lag} + \lambda, \\ 0, & \text{otherwise.} \end{cases} \quad (1)$$

$$\text{where } \gamma_{mlag} = \gamma_{max} - \frac{\gamma_{max}}{\lambda}(\dot{x}_{ego} - \dot{x}_{lag})$$

Note that if the EV is slower than the OV_{lag}, then $\gamma_{lag} = \gamma_{max}$, where γ_{max} is a design parameter that establishes the maximum possible acceleration for the EV during the merging maneuver. In case the EV is faster than the OV_{lag}, the value of γ_{lag} decreases linearly with respect to the speed difference, until it gets to 0 when $\dot{x}_{ego} > \lambda + \dot{x}_{lag}$, being λ a design parameter that adjusts the influence of the OVs on the EV acceleration. This implies that if the EV is significantly faster than OV_{lag} during the trajectory, it is not possible to increase its acceleration at that point.

Likewise, γ_{lead} considers the speed difference of the EV with respect to the leader vehicle:

$$\gamma_{lead} = \begin{cases} \gamma_{min}, & \text{if } \dot{x}_{lead} < \dot{x}_{ego}, \\ \gamma_{mlead}, & \text{if } \dot{x}_{lead} - \lambda \leqslant \dot{x}_{ego} < \dot{x}_{lead}, \\ 0, & \text{otherwise.} \end{cases} \quad (2)$$

$$\text{where } \gamma_{mlead} = \gamma_{min} - \frac{\gamma_{min}}{\lambda}(\dot{x}_{lead} - \dot{x}_{ego})$$

If the EV is faster than OV_{lead}, then γ_{lead} is set to γ_{min}, which is a design parameter that defines the maximum possible braking acceleration. If the EV is slower than OV_{lead}, the magnitude of γ_{min} decreases linearly until it gets to 0 when $\dot{x}_{ego} < \dot{x}_{lead} - \lambda$.

Finally, the acceleration $\ddot{x}_{ego}$ is obtained using the values of γ_{lag} and γ_{lead} and the gap distances with respect to both OVs:

$$\ddot{x}_{ego} = \begin{cases} \gamma_{lag}, & \text{if } x_{ego} < x_{lag} + B_{lag}, \\ \gamma_{mid}, & \text{if } x_{lag} + B_{lag} \leqslant x_{ego} < x_{lead} - B_{ego}, \\ \gamma_{lead}, & \text{otherwise.} \end{cases} \quad (3)$$

being B_{lag} the minimum safe gap between OV_{lag} and the EV, and B_{ego} the minimum safe gap between the EV and OV_{lead}, both computed using the second equation of motion:

$$B = d_c + \frac{\dot{x}^2}{2\gamma_{brake}} \tag{4}$$

where d_c is a parameter that defines the minimum possible separation between two vehicles; $\dot{x}$ is the speed of the vehicle of interest; and γ_{brake} is the maximum braking acceleration, which is γ_{min} for the EV and $\gamma_{min,OV}$ for the OV (a design parameter that defines the maximum acceleration considered safe for an external vehicle to apply during its driving).

If the EV is too close to OV_{lag}, then $\ddot{x}_{ego} = \gamma_{lag}$. If, on the contrary, the EV is too close to OV_{lead} a negative acceleration $\ddot{x}_{ego} = \gamma_{lead}$ is set. In any other case, the value of $\ddot{x}_{ego}$ is computed using a function with a minimum possible value of γ_{lead} and maximum possible value of γ_{lag}, as follows:

$$\gamma_{mid} = \gamma_{lead} \ + \alpha\,(\gamma_{lag} - \gamma_{lead}) \tag{5}$$

where α is defined as:

$$\alpha = 1 - \left(\frac{x_{ego} - G_{lag}}{G_{lead} - G_{lag}}\right)^3 \tag{6}$$

being $G_{lag} = x_{lag} + B_{lag}$ and $G_{lead} = x_{lead} - B_{ego}$ the limit positions of the lag and leader vehicles that respectively ensure safe gaps during the merging maneuver.

The term α defines the influence of γ_{lead} and γ_{lag} on $\ddot{x}_{ego}$ based on the distance with the OVs, i.e. if $(G_{lead} - G_{lag}) >> (x_{ego} - G_{lag}) \implies \alpha \to 1 \implies \gamma_{mid} \to \gamma_{lag}$, meaning that if the leader vehicle is further from the EV than the lag vehicle, the latter would have a larger influence on the acceleration of the EV, and vice versa. The motivation to use a cubic function for α is to obtain values more rapidly close to 1 when $(G_{lead} - G_{lag}) > (x_{ego} - G_{lag})$ than those obtained with a linear function. As a result, the influence of γ_{lag} is significantly increased on the merging acceleration. In the special case that OV_{lead} does not exist, then $\gamma_{lead} = 0$ and the term G_{lead} in (6) is replaced with $x_{ego} + \delta_{nl}$, where δ_{nl} is a design parameter which emulates a virtual leader vehicle at a fixed distance.

The merging profile $\mathbf{V}_{ego}$ is considered dangerous if the safe gap with respect to the leader or the lag vehicle cannot be guaranteed after the position-on-path of the EV is larger than the position-on-path of the yield line (x_{yl}). This danger condition δ can be formalized as follows:

$$\delta = (x_{ego} < G_{lag} \ \vee \ x_{ego} > G_{lead}) \ \wedge \ (x_{ego} > x_{yl}) \tag{7}$$

If the danger condition is met, the merging-before maneuver is aborted, and a new speed profile is created trying to merge after the lag-vehicle has passed the intersection point.

Fig. 6 shows a roundabout scenario where the EV is merging between a leader vehicle (blue) and a lag vehicle (red). The path candidates set $\mathcal{P}$ is plotted in green, and one of the candidates $\rho \in \mathcal{P}$ is highlighted in magenta. The initial state of the vehicles is detailed in Table I, where the initial position of the OV is computed with the virtual projection on the EV path at $t = 0$, using the PCPs.

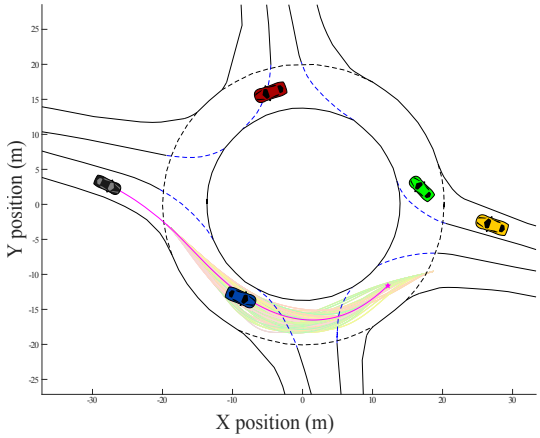

Fig. 6. Traffic status and path candidates for the merging-before example scene.

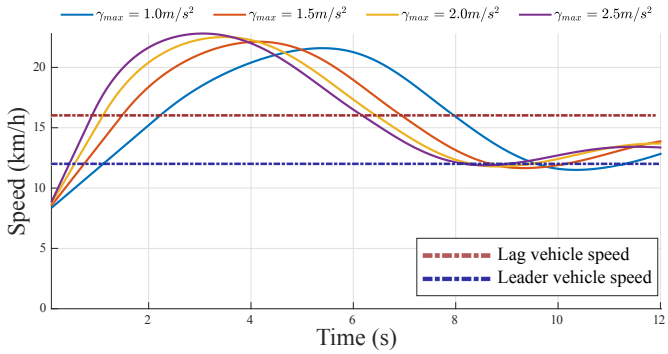

Fig. 7. Speed profiles for a single path candidate using different values of γ_{max} during the merging-before example scene.

TABLE I
INITIAL STATE OF VEHICLES FOR THE MERGING-BEFORE EXAMPLE SCENE.

Vehicle	Init. pos. on EV path (m)	Speed (km/h)
Ego-vehicle	0.0	8.0
Blue vehicle (Leader)	25.0	12.0
Red vehicle (Lag)	-15.0	16.0

For this case $N_{sp} = 4$, and a different value $\gamma_{max,i}$, $i \in 1 \ldots 4$ is used to generate each speed profile. Also, the position on path of the yielding line is $x_{yl} = 13.9m$. The configuration parameters are shown in table III.

Fig. 7 shows the resulting $\mathbf{V}_{ego,i}$ for ρ when different values of γ_{max} are used. The traveling speeds of $\dot{x}_{lag}$ and $\dot{x}_{lead}$ are also plotted.

For all $\mathbf{V}_{ego}$, the speed of the EV increases at the beginning of the merging maneuver, converging around V_{lead} at the end. This behavior is expected since $\mathbf{V}_{ego}(0) < \dot{x}_{lag}$, and therefore the value of γ_{lag} is large at first, generating higher values of $\ddot{x}_{ego}$ at the beginning of the maneuver. As the EV gets closer to OV_{lead}, $\dot{x}_{ego}$ becomes higher than $\dot{x}_{lag}$, so the value of γ_{lag} decreases, reducing the traveling speed. In order to show how the merging speed profile generation works, the limit speed profile Λ was not taken into account in this example, but in normal conditions the values of $\mathbf{V}_{ego}$ are limited by the magnitude of Λ, as described in [16].

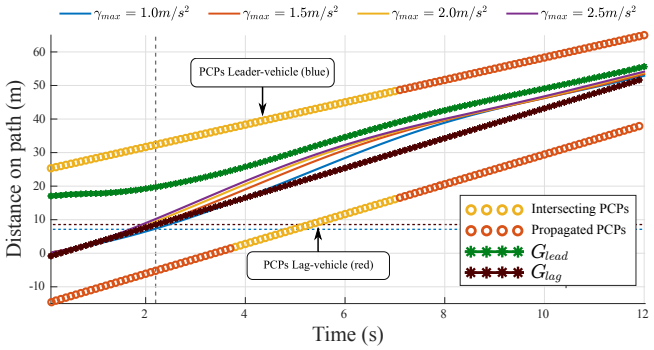

Fig. 8. Possible collision points and position-on-path evolution of the ego-vehicle for different values of γ_{max} for the merging-before example scene.

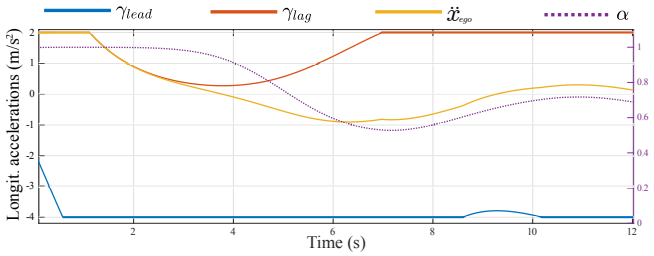

Fig. 9. Evolution over time of γ_{lead}, γ_{lag}, α and $\ddot{x}_{ego}$ for $\mathbf{V}_{ego,3}$.

The diversity on the resulting speed profiles is important to the decision making algorithm, because, in case the weights ω of the merit function (section II-A) are configured to prioritize utility, $\mathbf{V}_{ego,4}$ is more likely to be selected as the best trajectory. Conversely, if the weights are configured to prioritize longitudinal comfort, then the trajectory provided by $\mathbf{V}_{ego,1}$ would be preferred.

Fig. 8 shows the distance-on-path evolution for all $\mathbf{V}_{ego,i}$. The PCP for OV_{lag} and OV_{lead} are plotted using yellow and orange circles, using the same color code than Fig. 3b. The limit positions G_{lead} and G_{lag} are also depicted on the figure using green and brown bullets, respectively. It can be seen that all speed profiles maintain x_{ego} between the limit positions all along the trajectory, even at the end ($t > 10s$) when the gap becomes narrower. The only exception to this occurs for $\mathbf{V}_{ego,1}$, when $x_{ego} < G_{lag}$ at $t \approx 2.2s$ (red and blue dotted lines on Fig. 8), but since $x_{ego} < x_{yl}$ at that moment, the danger condition (7) is not triggered.

In the interest of showing the evolution over time of the parameters involved on the speed profile generation, as well as their interdependence and their roles on the process, Fig.9 shows the values of γ_{lead}, γ_{lag}, α and $\ddot{x}_{ego}$ for the generation of $\mathbf{V}_{ego,3}$. Since $\mathbf{V}_{ego,3}(0.6s) > V_{lead}$ then $\gamma_{lead} = \gamma_{min}$ from that moment, except on $t = [8.5s\,,\,10.1s]$. In the case of γ_{lag}, its value is lower than γ_{max} for $t = [1.1s\,,\,6.9s]$ when $\mathbf{V}_{ego,3} > V_{lag}$ (see Fig. 7). The evolution of the term α is plotted on a purple dotted line that uses the right hand vertical axis on the figure. It starts at $\alpha = 1$ because $x_{ego} \approx G_{lag}$ at the beginning of the maneuver, resulting on $\ddot{x}_{ego} = \gamma_{lag}$. As the EV moves away from G_{lag} and gets closer to G_{lead}, the value of α decreases, so γ_{lead} gets a larger influence on the value of $\ddot{x}_{ego}$, and the EV reduces its acceleration for $t > 3.5s$.

B. Merging after another vehicle

According to [13], human drivers tend to reduce the driving speed before the yield line without stopping completely when they are approaching a roundabout with traffic; this behavior allows to merge into the roundabout in a more efficient way after the OV has passed. Taking this into consideration, a limit speed profile (Λ) is generated with different restrictions such as a maximum lateral acceleration ($\gamma_{max,lat}$), maximum longitudinal acceleration (γ_{max}), minimum longitudinal acceleration for comfort ($\gamma_{min,com}$), initial speed (v_i), final speed (v_f), and a low-merging-speed restriction which imposes a speed value v_{yield} during a distance s_r before the yield line. The generation of Λ is performed by using algorithm 1. In the first step of the algorithm, the speed profile is computed by limiting the lateral acceleration according to the curvature of the path (using a circular motion equation). Then, the initial and final speeds of the profile are set. Next, the low-merging-speed restriction is applied to the path indexes before the yielding line. In the last section of the algorithm, the longitudinal acceleration is limited by verifying the speed variation between two consecutive points on the path (and modifying the speed if necessary). This process is repeated forwards and backwards to limit both positive and negative accelerations.

Algorithm 1 Restriction Speed profile.

Input: $(\kappa,\ v_i,\ v_f,\ v_r,\ i_{r0},\ i_{yl},\ d_p)$
Output: Λ

$\Lambda \leftarrow \sqrt{\frac{\gamma_{max,lat}}{|\kappa|}}$
$\Lambda_1 \leftarrow v_i$
$\Lambda_N \leftarrow v_f$
if $(i_{r0} >= 0)$ **then**
  $\Lambda_n \leftarrow v_r$ **for** $n = i_{r0}, ..., i_{yl}$
end if
for $n = 1$ to N **do**
  $\boldsymbol{a}_n \leftarrow \frac{\Lambda_n^2 - \Lambda_{n-1}^2}{2\,d_p}$
  if $(\boldsymbol{a}_n > \gamma_{max})$ **then**
    $\Lambda_{n+1} \leftarrow \sqrt{\Lambda_n^2 + 2\,\gamma_{max}\,d_p}$
    $\boldsymbol{a}_n \leftarrow \gamma_{max}$
  end if
end for
for $n = N$ to 1 **do**
  $\boldsymbol{a}_n \leftarrow \frac{\Lambda_n^2 - \Lambda_{n-1}^2}{2\,d_p}$
  if $(\boldsymbol{a}_n < \gamma_{min,com})$ **then**
    $\Lambda_n \leftarrow \sqrt{\Lambda_{n+1}^2 + 2\,\gamma_{min,com}\,d_p}$
    $\boldsymbol{a}_n \leftarrow \gamma_{min,com}$
  end if
end for
return Λ

The inputs of the algorithm are the curvature κ of a candidate path ρ; the final speed v_f, derived from the road curvature; the restriction speed to apply before the yield line v_r; the index i_{r0} of the node on the path where speed restriction must start, located at a position on path $x_{r0} = x_{yl} - s_r$; the index i_{yl} of the node on the path where there is an intersection with the yield line, and the distance d_p used to discretize the Bézier

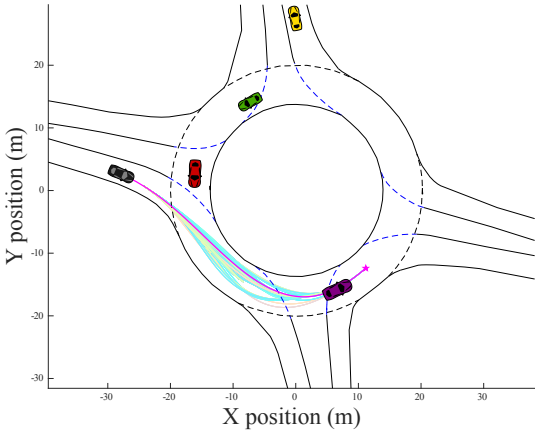

Fig. 10. Traffic status and path candidates for the merging-after example scene.

curves of $\mathcal{P}$. In case there is no yield line on the scene, or the speed restriction before the yield line is not required i.e. during the merging-before maneuver, the values of i_{r0} and i_{yl} are set to -1.

Once the limit speed profile Λ is computed, the dynamic speed profile $\mathbf{V}_{ego}$ may be generated. To this purpose, the algorithm proposed in [16] is implemented with a single variation: to discard the PCPs of the OV inside the roundabout while $x_{ego} < x_{yl}$. The feasibility of the maneuver is evaluated checking the gap between the closest PCP and the position of the EV at the time the yield line is reached (t_{yl}), as follows:

$$\delta = \min(PCP_{t=t_{yl}}) < (x_{ego} + B_{ego}) \tag{8}$$

If the danger condition becomes true, the merging-after profile is not feasible and a stop-on-yield-line maneuver is performed. If the gap is safe, the speed profile for $x_{ego} > x_{yl}$ is generated using the inter-distance model.

Fig. 10 shows a driving scene where the ego-vehicle is merging into a roundabout with three vehicles inside. The initial state of the vehicles on the scene is displayed on table II.

TABLE II
INITIAL STATE OF VEHICLES FOR THE MERGING-AFTER EXAMPLE SCENE.

Vehicle	Dist. on EV path (m)	Speed (km/h)
Ego-vehicle	0.0	18.2
Purple vehicle	29.5	24.4
Red vehicle	1.2	27.9
Green vehicle	-8.6	14.3

The position on path of the yielding line is $x_{yl} = 13.9m$; the parameters used for the generation of $\mathbf{V}_{ego}$ are depicted in table III.

The speed profile for this maneuver is displayed on Fig. 11 and the position-on-path evolution is shown on Fig. 12. A merging maneuver before OV_{red} is not possible since the back-propagated PCP show an initial position higher than $0m$ (Fig. 12), so it is not considered as a lag vehicle. On the other hand, a merging maneuver between OV_{red} and OV_{green} was not possible to find, since the danger condition (7) was

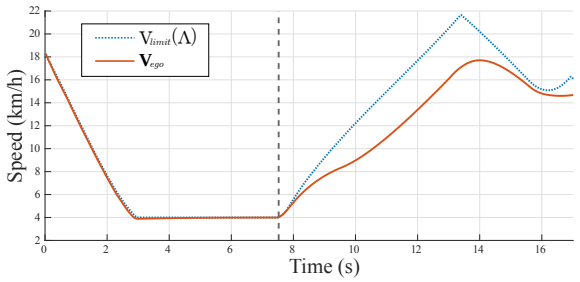

Fig. 11. Limit speed profile Λ and final speed profile $\mathbf{V}_{ego}$ during the merging-after example scene.

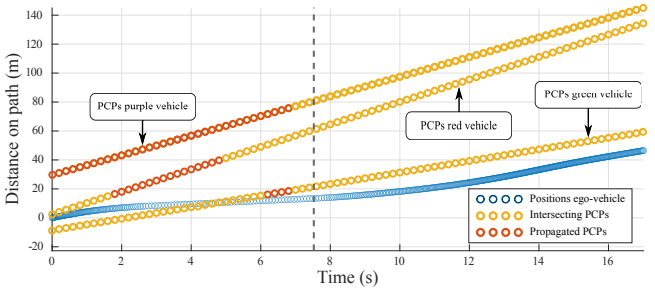

Fig. 12. Possible collision points of the OVs and position-on-path evolution of the ego-vehicle for the merging-after example scene.

triggered for all the generated profiles. Hence, the generated maneuver attempts to merge into the roundabout after OV_{green} has crossed the intersection point.

As can be observed in Fig. 11, the limit speed profile Λ (blue dotted line) sets the restriction speed to $v_{yield} = 4km/h$ for the segment of the path $s = [7.9m : 13.9m]$. By the time the EV reaches x_{yl} (marked with a vertical dashed line at $t_{yl} = 7.7s$ both in Fig. 11 and Fig. 12), the closest PCP position is $min(PCP_{t=t_{yl}}) = 22.3m$ (due to OV_{green}). In this case, the maneuver is considered feasible since the danger condition (8) is not triggered because $22.3m > 13.9m + 7.26m$. If the danger condition is triggered, the speed profile is discarded and a stop-on-yield-line maneuver would be generated. The speed profile for $t > t_{yl}$ is generated using the inter-distance model proposed in [16], to maintain a safe distance with respect to the PCP of the last OV, while meeting comfort constraints (i.e. $\mathbf{V}_{ego} < \Lambda$).

In the special case there is no OV present inside the roundabout, the speed profile is generated using the algorithm described on this section, but instead of using the restriction parameter v_r, a larger restriction parameter v_{rf} is used.

C. Stopping on yield line

The last option, when it is not possible to merge before or after another vehicle on the roundabout, is to stop the vehicle on the yield line and wait for a gap large enough to merge into the roundabout. The speed profile to stop on the yield line is generated using Algorithm 1. In this specific case, $v_r = 0m/s$ and the index i_{r0} is computed using a distance $s_r = 4m$, so that the EV stops at a safe distance from the roundabout ring.

(a) (b)

Fig. 13. Aerial view of the testing roundabouts of openDD. (a) Roundabout rdb_4. (b) Roundabout rdb_7.

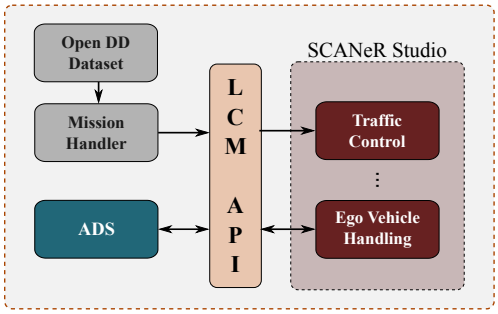

Fig. 14. Software architecture used to run realistic traffic scenes on a SiL simulation

IV. Experimental Results

This section details the experimental setup used to validate the performance of the TG using the described merging strategy for roundabouts; it also describes the experiments and analyses the obtained results. Two types of experiments were designed and executed:

- Recreate a merging maneuver from a public dataset in a simulation environment to evaluate the performance of the TG and compare it with (i) a real human-driven vehicle and (ii) a state-of-the-art technique.
- Generate different traffic scenes by randomly modifying the driving speed of the OVs from the original dataset scenes. Then, evaluate the robustness of the algorithm when facing these traffic conditions.

The experiments were conducted on two of the roundabouts available on openDD: rdb_4 and rdb_7. The first roundabout has a radius of 22m, while the latter has a radius of 18.5m. Fig. 13 shows an aerial view of the used roundabouts.

The configuration parameters used during the experiments are shown in table III.

TABLE III
Configuration Parameters.

Parameter	Value	Units
γ_{max}	2.5	m/s^2
$\gamma_{min,com}$	-2	m/s^2
$\gamma_{max,lat}$	2.5	m/s^2
γ_{min}	-4	m/s^2
$\gamma_{min,OV}$	-1.5	m/s^2
λ	1.38	
v_r	5	km/h
v_{rf}	15	km/h
s_r	14	m
dc	6	m
δ_{nl}	15	m

A. Experimental setup

The TG was tested using a software-in-the-loop (SIL) simulation environment. The simulation software used is SCANeR Studio 1.9 [23], which contains the tools and models to build virtual scenarios including infrastructure, road environment, vehicles, and traffic. The driving scenarios created in SCANeR for this work are real traffic scenes obtained from the dataset openDD. In order to replicate the driving scenes from the dataset on the simulator, a software module named Mission handler was implemented. It is able to read vehicles state from a selected scene of the dataset and transmit traffic commands to the vehicles on the simulator. The modular architecture of SCANeR Studio requires different modules working in parallel to run a simulation, in this framework, two customized modules were developed (i) to control the vehicles transmitted by the Mission handler and (ii) to handle the ego vehicle on the simulation. The data transmitted from the Mission Handler to the simulator and the data shared between the ADS and the simulator is handled by a customized Lightweight Communications and Marshalling (LCM) API (a detailed description of this API is depicted on [24]). Using this approach it is possible to test the TG in a closed loop architecture, where, even though the virtual vehicles are set to have the same behavior as the ones on the dataset, they have the ability to react to the EV's behavior during the simulation. This architecture is shown in Fig. 14.

B. Human driving comparison

Different driving scenes were selected from the dataset. For each of them, one of the vehicles present on the scene was selected as the Vehicle of Interest (VoI), which was used as baseline to evaluate the performance of the TG. The criteria used to select the driving scenes were: (i) the VoI must start at an initial distance larger than 30m from the roundabout, (ii) there must be no vehicle between the VoI and the roundabout, (iii) the VoI of the dataset must merge into the roundabout without stopping on the yielding line. Once the traffic scenes were selected from the dataset, they were recreated on the simulator and the TG was tested using different configurations of the weights for the merit function. Five different configurations were tested, each one the first four prioritize a different DV (see section II-A) over the others, while the fifth one has a balanced configuration. The test runs of the TG were compared to the human driving from the dataset using six performance indicators presented on table IV.

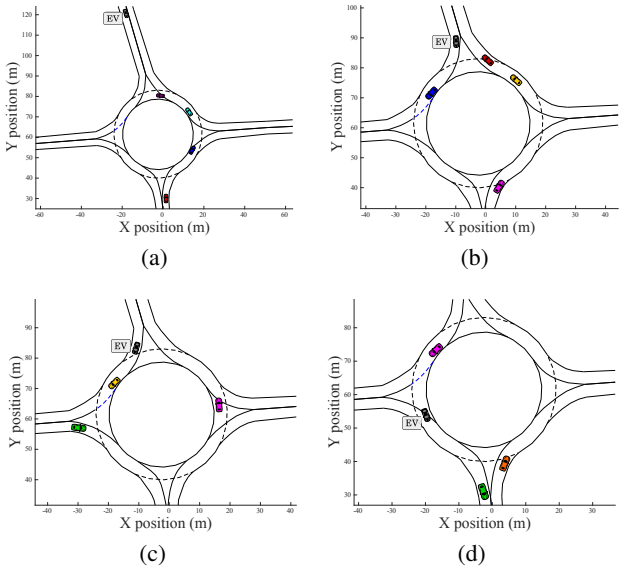

Fig. 15. Time evolution of the traffic scene in rdb$_4$. (a) traffic status at $t = 1s$. (b) traffic status at $t = 9s$ (c) traffic status at $t = 13s$ (a) traffic status at $t = 19s$.

TABLE IV
PERFORMANCE INDICATORS.

Parameter	**Formula**
Longitudinal Acceleration	$max(\|\gamma_x(s)\|)$
Longitudinal Jerk	$\overline{\jmath_x(s)}$
Lateral Acceleration	$max(\|\gamma_y(s)\|)$
Lateral Jerk	$\overline{\jmath_y(s)}$
Risk to collision	$\overline{RTTCE} + max(RTTCE)$
Travel time	t_N

All the performance indicators are computed offline using the resulting trajectory of the vehicle and the position of the obstacles during the test run. The longitudinal/lateral acceleration indicators measure the maximum acceleration value during the test run; the longitudinal/lateral jerk indicators measure the average value of the jerk. To calculate the risk to collision indicator, the Risk from Time to Close Encounter (RTTCE) metric proposed in [25] is computed during the complete trajectory with respect to the OV present on the scene. The considered metric uses a sum of the maximum risk value over the trajectory and the average risk value. Finally, the travel time indicates how much time the vehicle needed to get to the goal position.

In the first selected traffic scene, extracted from rdb$_4$, the VoI starts 49m away from the roundabout with an initial speed $v_{voi} = 39km/h$, then it slows down as it gets closer to the roundabout and it merges between two vehicles without stopping on the yield line. Fig. 15 shows in 4 snapshots the evolution of this traffic scene. The total distance completed by the VoI (black vehicle) is 102m.

The speed profiles of the five tests on autonomous mode and the human-driven test are shown in Fig. 16. It can be seen that both the human and the TG reduce the traveling speed

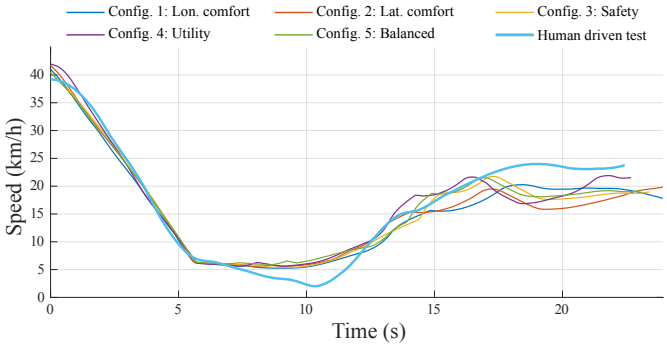

Fig. 16. Speed profiles for the test runs on the traffic scene of rdb$_4$.

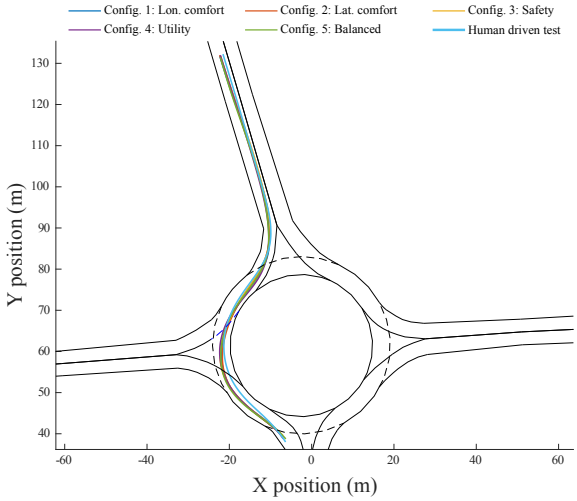

Fig. 17. Final paths for the test runs on the traffic scene of rdb$_4$.

when approaching the roundabout, maintaining afterwards a low speed from $t \approx 6s$, to finally increase the speed to merge into the roundabout at $t \approx 11s$. In the case of the TG the EV keeps a constant speed before merging, while the human pilot keeps slowing down as he gets closer to the yield line. When the merging maneuver is performed, the acceleration of the human pilot is higher than the acceleration of the TG test runs, as it has to start from a lower speed.

The complete paths followed by the EV and the VoI during all the test runs on the scenario rdb$_4$ are shown on Fig. 17. It can be seen that the paths of the TG are very similar to the human driver's path during the merging maneuver of the roundabout, but once inside the roundabout ring, the TG made wider curves than the human, reducing thus the lateral acceleration.

The six performance indicators from the TG test runs and the human-driven test run are shown in the radar plot on Fig. 18. The definition of the KPIs of table IV implies a smaller-is-better (SiB) standard. In other words, the closer to the center of the radar, the better the performance under consideration. In general, the performance of the TG with the different weight configurations is similar to the human pilot's. Regarding the longitudinal acceleration indicator, the TG showed better performance on all the configurations; the reason for this is that the largest values of the longitudinal ac-

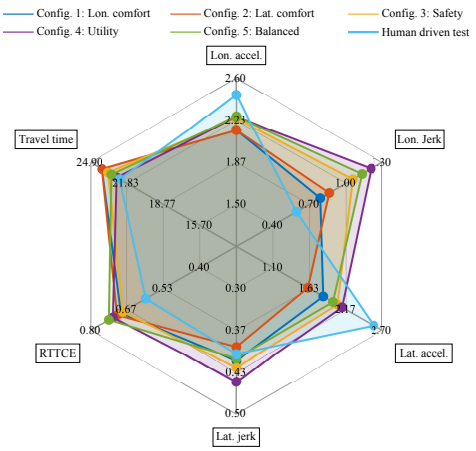

Fig. 18. Performance indicators for different test runs on traffic scene of rdb_4.

celeration were presented on the initial braking at $t = [0s, 6s]$, and during this period of time, the human pilot applied more deceleration than the TG. In terms of the lateral acceleration, the TG kept its speed lower and made wider curves than the human pilot, obtaining a more comfortable trajectory, but penalizing the travel time, where the human pilot presented better performance. Indeed, it reached the destination 0.68s faster than the fastest test run of the TG (configuration 4). In the case of the longitudinal jerk, the human pilot outperformed the TG, probably due to the transition from the initial braking status to the speed restriction on $t \approx 6s$, where the TG changes its acceleration in a more sudden way than the human. Regarding the RTTCE indicator, the highest risk measure is obtained when the EV is about to merge into the roundabout. Since the TG started the merging maneuver before the human pilot, and also at a higher speed, it exhibited higher risk values.

Fig. 19 shows the gap distances of the test runs regarding the leader and the lag vehicles during the merging maneuver. This gaps are computed from the moment the vehicle crosses the yield line until it gets completely into the roundabout-ring. For this traffic scene, the average gap with respect to the leader vehicle while merging was 24.1m and the average gap with respect to the lag vehicle was 23.2m. The TG kept larger gaps from the leader vehicle than the human pilot on average, being the largest gaps for configurations 1, 2 and 3 (which prioritized comfort and safety). The gaps with respect to the lag vehicle were smaller for the TG test runs than for the human-driven test run, being the smallest gap for the configuration 1 (20.3m).

The second scenario was located on rdb_7. The TG was also tested in this scenario with five configurations for the weights of the decision variables of the merit function. In this case, the VoI starts 31m away from the roundabout and its initial speed is $v_{voi} = 35km/h$. It also slows down as it gets closer to the roundabout and then it merges between two vehicles, but the gap between the vehicles on the roundabout during the merging maneuver is narrower than the gap of the first scenario. Fig. 20 shows the evolution of this traffic scene (the VoI is plotted in black). At $t = 1s$ (Fig. 20a), the VoI is approaching to the roundabout with high traffic. At $t = 4s$ (Fig. 20b), the VoI reduces its speed and is waiting for a

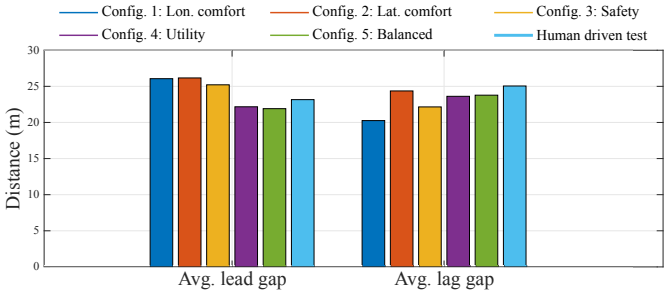

Fig. 19. Lead and lag gaps for different test runs on traffic scene of rdb_4.

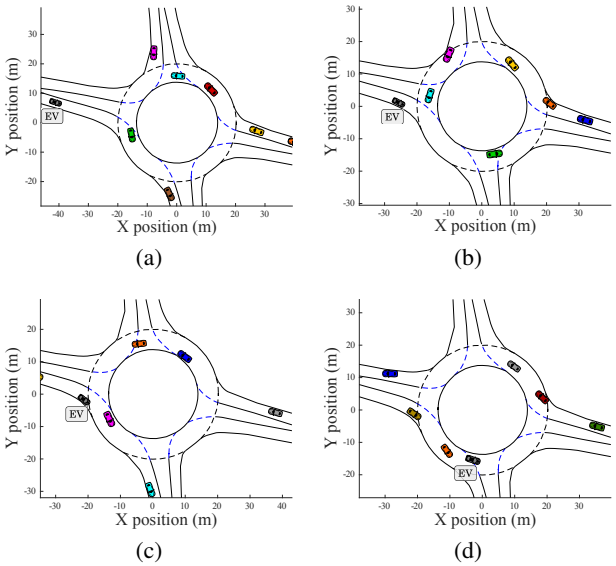

Fig. 20. Time evolution of the VoI on a merging scene in rdb_7. (a) Traffic status at $t = 1s$. (b) Traffic status at $t = 4s$ (c) Traffic status at $t = 8s$ (d) Traffic status at $t = 13s$.

possible merging gap. At $t = 8s$ (Fig. 20c), the VoI is merging after the magenta vehicle has passed the intersection point and before the cyan vehicle reaches that point. Finally, at $t = 13s$ (Fig. 20d) the VoI is completely merged into the roundabout. The total distance traveled by the EV in this scenario is 132m.

The speed profiles of the five TG test runs and the human-driven test run are shown in Fig. 21. It can be seen that the TG reduces the speed before the human pilot when approaching to the roundabout (due to the value of s_r), then, the TG maintains a traveling speed $v_{ego} = 6km/h$ from $t \approx 4s$ while the human pilot reduces its speed down to $v_{ego} = 2km/h$ during this lapse. Both agents (TG and human pilot) increase their speed to merge into the roundabout at $t \approx 11s$. After the merging is completed, the human pilot keeps increasing its speed while crossing the roundabout, while the TG reduces its speed at $t \approx 15$ to guarantee comfort constraints.

The complete paths followed by the VoI and the EV and during all the test runs on the rdb_7 are shown on Fig. 22. The paths generated by the TG were again similar to the human driver's path around the merging point of the roundabout. In addition to that, the TG made also wider curves than the human before exiting the roundabout.

Fig. 23 shows the comparison between the TG test runs

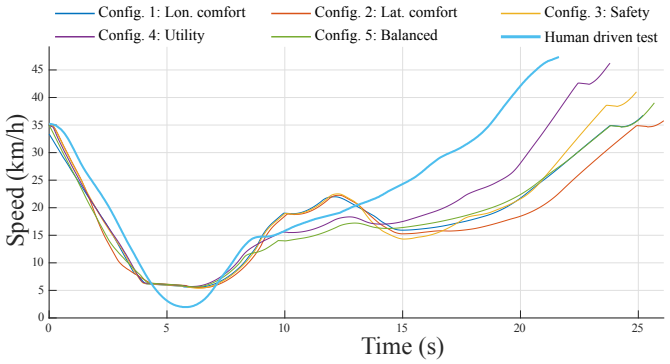

Fig. 21. Speed profiles for different test runs on traffic scene of rdb_7.

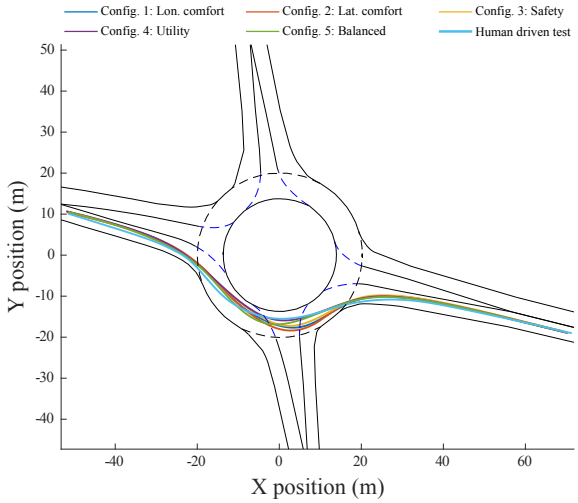

Fig. 22. Paths for different test runs on traffic scene of rdb_7.

and the human driven test run for the scenario of rdb_7. In general, the performance of this human pilot was slightly better than the TG performance. The high values of the longitudinal acceleration of the TG are due to the initial conditions of the experiment; since the EV starts 31m away of the yield line, the TG has to brake firmly in order to get to v_r before reaching s_r. Under normal operation conditions, where the TG is in control of the EV since it starts to move, it would have started to brake before in order to keep the longitudinal acceleration bounded. In spite of this particular situation, the difference between the maximum longitudinal acceleration between a human and the TG for configuration 5 was only $0.16m/s^2$. For the longitudinal jerk, it can be observed that the human pilot performs a smoother driving, reducing its speed before merging at $t = 8s$. This transition is sharper with the TG, creating higher jerk values. Regarding the lateral acceleration, the human pilot obtained a lower value than the TG, but it was only $0.25m/s^2$ in average. The TG reduced its speed once on the roundabout to meet the lateral acceleration restriction, while the human pilot was able to follow a path that allowed him (her) to keep accelerating inside the roundabout, getting to the destination 2.16s faster than the fastest configuration of the TG. For this scenario the human pilot started accelerating before the TG to perform the merging maneuver. As a result, the risk of collision with the leader vehicle (magenta on Fig. 20c) increased, leading to a worse performance on the RTTCE for the human pilot.

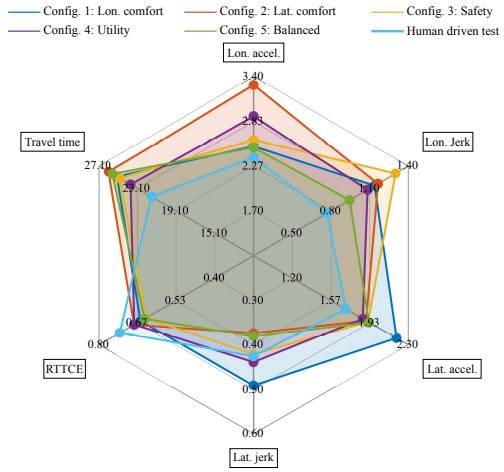

Fig. 23. Performance indicators for different test runs on traffic scene of rdb_7.

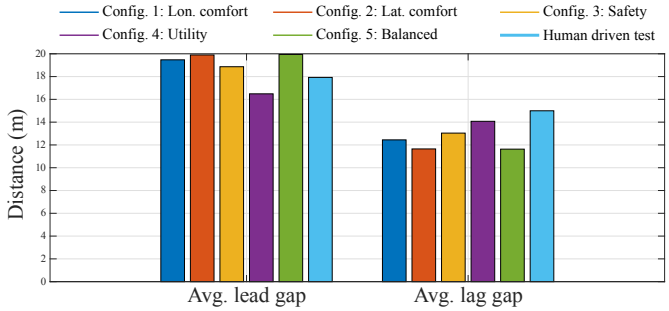

Fig. 24. Lead and lag gaps for different test runs on traffic scene of rdb_7.

The average gap values for the merging maneuver on the second driving scenario are shown on Fig. 24. For this scenario, the gaps with respect to the leader vehicle were higher for TG test runs (18.93m avg.) compared with the human pilot's (17.92m). Conversely, the gaps with respect to the lag vehicle were lower for the TG (12.56m avg.) compared to the human (14.99m). Note that although the gap values to the lag vehicle were smaller, they were still higher than the minimum safety gap obtained from (4) for the lag vehicle (9.28m for a speed of 11.3 km/h). This tight gap values show that the TG is capable of performing merging maneuvers in crowded scenarios.

C. Testing on multiple modified scenarios

In order to test the TG in several situations, a new set of 25 driving scenarios was created from each of the testing scenarios of section IV-B. The navigation speeds of all OV on the original driving scene were randomly modified using a normal distribution with a standard deviation $\sigma = 8\,km/h$. Then, the TG was tested on each scenario using the configuration with balanced weights of the DV. These variations allow the EV to deal with a variety of situations, such as merging before OVs at different speeds, performing a merging maneuver without reducing the speed, or yielding because merging before another vehicle is not safe.

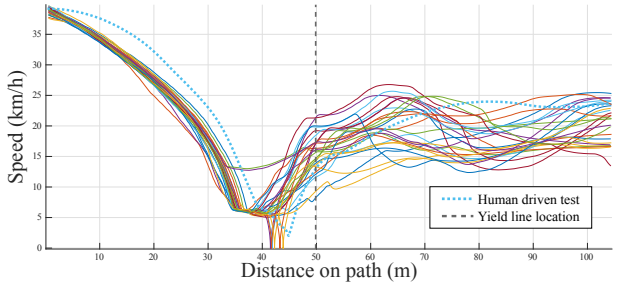

Fig. 25. Speed profile along the path for the TG test runs on the modified scenarios of rdb_4.

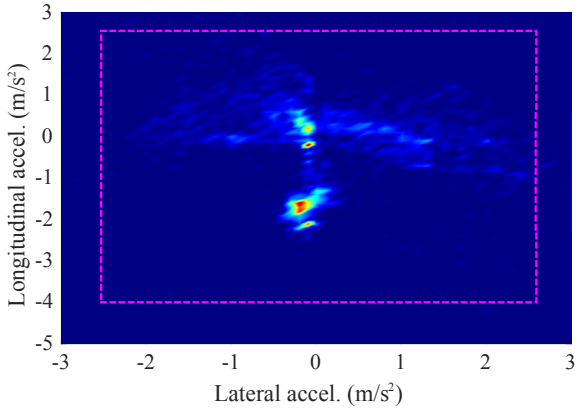

Fig. 26. Density graph of the ego-vehicle acceleration during the TG test runs on the modified scenarios of rdb_4.

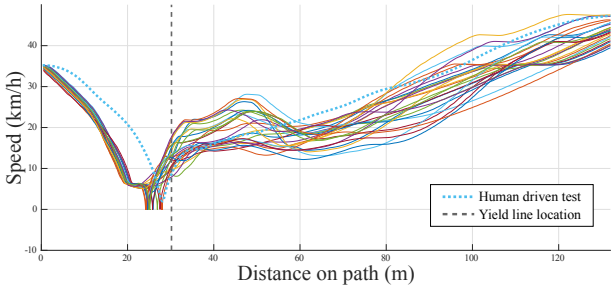

Fig. 27. Speed profile along the path for the TG test runs on the modified scenarios of rdb_7

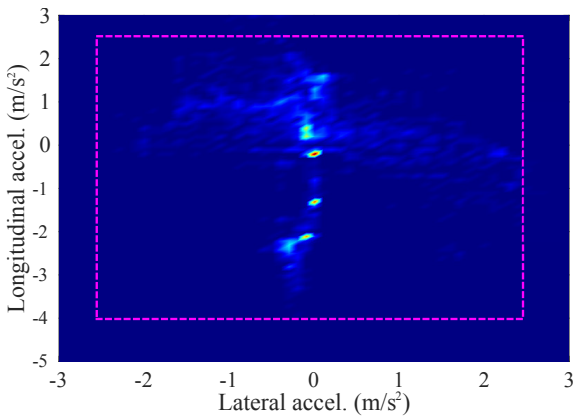

Fig. 28. Density graph of the ego-vehicle acceleration during the TG test runs on the modified scenarios of rdb_7.

The speed profiles along the path for the different test runs on the modified versions of the rdb_4 scenario are shown on Fig. 25. As waiting times vary from one experiment to another, data is plotted along the path (and not versus time), improving thus the readability of the figure. The human driven test run from the original dataset is plotted only as a reference for the reader (as a dotted cyan line) and the position of the yield line is also plotted on the figure (black dashed line).

All the experiments were handled safely. The TG performed a merging maneuver without stopping on 19 out of the 25 scenarios, two of which started the merging maneuver at $v_{ego} \approx 13km/h$. When the merge-after maneuver was executed, the limitation speed v_r was reached at 35m in most of the cases, as expected, since the initial distance to the yield line is 49m and the restriction distance $s_r = 14m$. In 6 specific scenarios the EV stopped before the yield line at a safe distance from it; the minimum and maximum stop distance to the yield line were $d_{stop} = [5.7m\,,\, 8.1m]$.

Fig. 26 shows a heat map of the longitudinal and lateral accelerations of all test runs. It can be observed that the accelerations were bounded to the design limits of Table III. Note that the zone around $\gamma_x = -2m/s^2\,,\, \gamma_y = 0m/s^2$ is repeated at the beginning of all the experiments when approaching to the roundabout, that is why it has a large density value.

The speed profiles along the path for the 25 test runs on the modified versions of the rdb_7 scenario are shown on Fig. 27. The human pilot run is plotted as a reference for the reader (dotted cyan line) and the position of the yield line is plotted as a black dashed line at 45m.

All test runs using the TG slow down before the human due to the restriction distance set by design. In this case, the TG stopped on the yield line on 16 out of the 25 scenarios. And it was able to merge into the roundabout without stopping on the remaining 9. This can be explained because the selected scenario of rdb_7 had more vehicles (17 total) than the scenario of rdb_4 (10 total), leading to tighter merging gaps and a more challenging merging scenario. Despite this, all the scenario variations were safely resolved, being the minimum and maximum stop distance to the yield line $d_{stop} = [3.01m\,,\, 6.94m]$.

Fig. 28 shows the density graph of the longitudinal and lateral accelerations of all test runs of rdb_7. Again, the accelerations were bounded to the design limits of Table III. Nevertheless, in this scenario the accelerations were more spread than in the previous one.

D. Comparative experiments

The Fictitious Acceleration based Merging Strategy (FAMS) described in this work was compared to the strategy proposed in [2], where virtual instances of the OVs and their corresponding occupancy intervals are used for finding a safe gap during a roundabout insertion maneuver. This technique was selected to perform the comparative for two main reasons: (i) it was validated with realistic traffic with multiple OVs on roundabouts (which is the scope of this paper); and (ii) its speed profile generation algorithm takes into account the state of the OVs. This technique will be referred to as VIIM

(Virtual Instance based Insertion Maneuver) on the remaining of this document. The parameters involved in the computation of the merging gap (A, α, d_{safe}) were selected heuristically to guarantee a safe merging gap in all the driving scenarios where the algorithm was tested without significantly impacting on its merging capacity. The parameter v_n, which defines the maximum travel speed, was set so that the lateral acceleration is bounded while driving through the roundabout. (table V) shows the numerical values of all these parameters).

TABLE V
CONFIGURATION PARAMETERS OF VIIM STRATEGY.

Parameter	Value	Units
A	8	N.A.
α	0.5	N.A.
d_{safe}	10	m
v_n	25	km/h

Both algorithms were tested in the same 25 driving scenarios of rdb_4 presented in section IV-C, but some initial conditions were modified to allow the merging algorithms to approach the roundabout without any influence of the EV initial position. More specifically, the initial speed of the EV and the distance to the roundabout were modified to $v_{ego,0} = 15$ km/h and 77m, respectively. Fig. 29 shows the speed, the longitudinal acceleration and the lateral acceleration along the path of each algorithm for all the experiments. The experiments of FAMS algorithm are plotted in blue, while experiments of VIIM algorithm are plotted in orange.

In Fig. 29a it can be seen that the speed profiles of FAMS algorithm were more consistent during the tests; they start to brake around 40m before the yielding line until $v_{ego} \approx v_r$, where they decide whether to merge or to yield into the roundabout. VIIM algorithm approaches the roundabout at nominal speed v_n and starts to brake approximately at 15m before the yielding line if it detects the gap is not large enough, or, in case the gap is safe, it merges at faster speeds than FAMS algorithm. This is a significant difference, since having a low speed before merging allows to perform a yielding maneuver safely in case a new OV is suddenly detected. Once the EV is inside the roundabout, the FAMS algorithm is slower than VIIM algorithm, as the first one takes into account different comfort restrictions, while the latter drives at $\dot{x}_{lead}$ if $OV_{lead} \neq \varnothing$ or at v_n otherwise. Regarding the longitudinal acceleration, it can be observed that the FAMS algorithm breaks at $\ddot{x}_{ego} \approx -1m/s^2$ to approach the roundabout; then, if it decides to yield, it brakes at $\ddot{x}_{ego} \approx -2.3m/s^2$. In the case of VIIM algorithm, it starts to brake at $\ddot{x}_{ego} \approx -2m/s^2$ when yielding, getting close to $\ddot{x}_{ego} \approx -4m/s^2$ before stopping. The positive acceleration to merge into the roundabout is similar in both algorithms. Regarding the lateral acceleration, it can be observed that it is more contained for the FAMS algorithm due to the comfort restrictions of Λ; however, VIIM algorithm presented higher lateral accelerations when crossing the roundabout because the only restrictions were v_n and $\dot{x}_{lead}$.

When approaching the roundabout, the EV always reaches a point where it has to decide to merge without stopping or to yield. If the EV stops completely before merging, it is more difficult to find a safe gap to merge due to the large relative speeds with respect to the vehicles driving on the roundabout ring. As a result, the waiting times may be very large in high-traffic scenarios. Fig. 30 shows the waiting times on the stop line (once the EV has yielded) for both algorithms in each driving scenario.

One of the main differences between FAMS and VIIM algorithms is that the first one generates a speed profile that may accelerate to keep a safe gap with respect to OV_{lag}, while the latter considers a constant speed on both vehicles to decide if the gap is safe enough to merge. The possibility to accelerate allowed the FAMS algorithm to merge without stopping in 14 out of 25 experiments, while the VIIM algorithm performed this maneuver only 6 out of 25 experiments. This feature also affects the waiting times while stopped, since the average

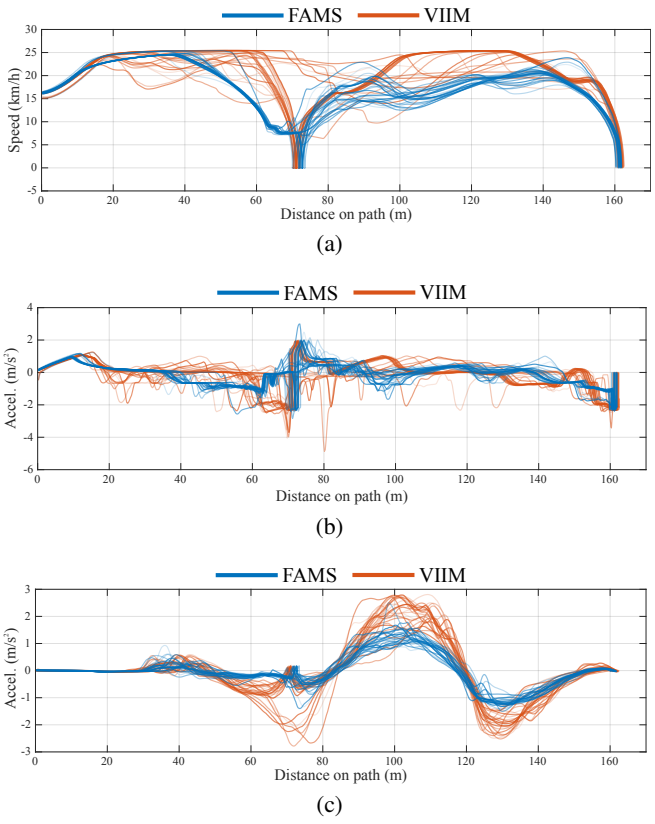

Fig. 29. Comparison of the EV dynamic variables during the experiments of FAMS and VIIM algorithms. (a) Longitudinal speed. (b) Longitudinal acceleration. (c) Lateral acceleration

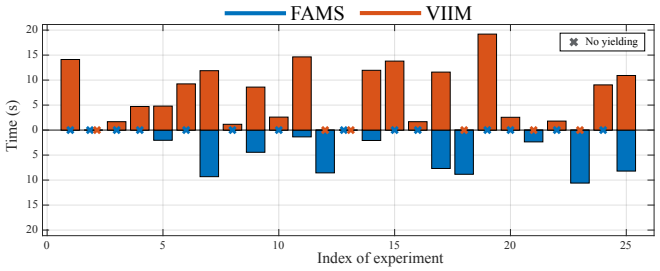

Fig. 30. Waiting times while yielding.

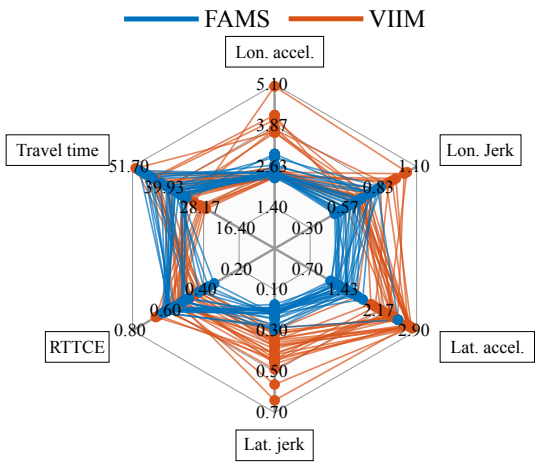

Fig. 31. Performance indicators for the different merging strategies on the modified scenarios of rdb_4.

waiting time for the FAMS algorithm (5.95s) was smaller than the average waiting time of VIIM algorithm (8.21s).

Fig. 31 shows the performance indicators for all the experiments carried out with each algorithm. It can be observed that the FAMS algorithm presented a better behavior on the four comfort-related indicators (accelerations and jerks). This difference can be explained by the differences in traveling speed of each algorithm, as discussed in the analysis of Fig. 29. Regarding the RTTCE indicator, both algorithms presented similar performances, with average values of 0.51 and 0.54 with VIIM and FAMS, respectively; these values of RTTCE represent no risk during the merging maneuver and are similar to the risk magnitude of the human drivers analysed in section IV-B. Respecting the travel time indicator, the VIIM algorithm achieved the fastest experiments when it was able to merge in the roundabout without stopping, presenting an average time of $t_{VIIM,merge} = 28.9s$ for these experiments versus an average time of $t_{FAMS,merge} = 37.4s$ for the FAMS algorithm. However, the travel time for the experiments that yielded on the stop line was more reduced with FAMS than with VIIM, obtaining average times of $t_{FAMS,yield} = 38.1s$ and $t_{VIIM,yield} = 40.5s$, respectively.

V. Conclusion

A speed profile generation algorithm to merge into roundabouts was proposed in this paper. The proposed strategy prioritizes the time-efficient merging maneuvers, while maintaining safety and comfort constraints.

The algorithm was validated on a SiL-simulation environment where the driving scenes were recreating open datasets. This setup allows to reproduce naturalistic environments, while guaranteeing that all the surrounding driving agents can dinamically adjust their behavior according to the evolution of the TG behavior.

An evaluation framework was implemented to evaluate the performance of the TG and compare its results with human driven data under the same environment. The comparison showed that the TG was able to handle real-traffic situations similarly to human drivers on different performance indicators like maximum longitudinal and lateral accelerations, average jerk values, time to close encounter with OV or travel time.

To assess the robustness of the merging algorithm under different driving conditions, modified versions of the roundabout scenarios were built. The system was able to handle safely all driving scenarios and was able to maintain the comfort constraints. Lastly, the performance of the algorithm was compared with another state-of-the-art insertion maneuver strategy.

The merging-before speed profile generation proposed in section III-A may be easily applied to other merging scenarios an AV may encounter, like ramp merging on highway or lane changing with traffic. Future work will be oriented towards the deployment and evaluation of the TG performance in these driving situations, both in simulation and with a real automated car.

Acknowledgments

This work has been partially funded by the Spanish Ministry of Science and Innovation with the National Project NEWCONTROL (PCI2019-103791), the Community of Madrid through SEGVAUTO 4.0-CM Programme (S2018-EMT-4362), and by the European Commission and ECSEL Joint Undertaking through the Project NEWCONTROL (826653).

References

[1] M. Morsali, E. Frisk, and J. Åslund, "Spatio-temporal planning in multi-vehicle scenarios for autonomous vehicle using support vector machines," *IEEE Transactions on Intelligent Vehicles*, vol. 6, no. 4, pp. 611–621, 2021.

[2] S. Masi, P. Xu, and P. Bonnifait, "Roundabout crossing with interval occupancy and virtual instances of road users," *IEEE Transactions on Intelligent Transportation Systems*, vol. 23, no. 5, pp. 4212–4224, 2022.

[3] W. Zhan, C. Liu, C.-Y. Chan, and M. Tomizuka, "A non-conservatively defensive strategy for urban autonomous driving," in *Proceedings IEEE International Conference on Intelligent Transportation Systems (ITSC)*, 2016, pp. 459–464.

[4] T. Stanger and L. del Re, "A model predictive cooperative adaptive cruise control approach," in *2013 American Control Conference*, 2013, pp. 1374–1379.

[5] G. Guo, D. Yang, and R. Zhang, "Distributed trajectory optimization and platooning of vehicles to guarantee smooth traffic flow," *IEEE Transactions on Intelligent Vehicles*, pp. 1–1, 2022.

[6] A. Danesh, W. Ma, C. Yu, R. Hao, and X. Ma, "Optimal roundabout control under fully connected and automated vehicle environment," *IET Intelligent Transport Systems*, vol. 15, no. 11, pp. 1440–1453, 2021.

[7] B. Filocamo, J. A. Ruiz, and M. A. Sotelo, "Efficient management of road intersections for automated vehicles - the frfp system applied to the various types of intersections and roundabouts," *Applied Sciences*, vol. 10, no. 1, pp. 1–25, 2020.

[8] A. S. M. Bakibillah, M. A. S. Kamal, C. P. Tan, S. Susilawati, T. Hayakawa, and J.-i. Imura, "Bi-level coordinated merging of connected and automated vehicles at roundabouts," *Sensors*, vol. 21, no. 19, pp. 1–15, 2021.

[9] P. Hang, C. Huang, Z. Hu, Y. Xing, and C. Lv, "Decision making of connected automated vehicles at an unsignalized roundabout considering personalized driving behaviours," *IEEE Transactions on Vehicular Technology*, vol. 70, no. 5, pp. 4051–4064, 2021.

[10] D. González, J. Pérez, and V. Milanés, "Parametric-based path generation for automated vehicles at roundabouts," *Expert Systems with Applications*, vol. 71, no. 1, pp. 332–341, 2017.

[11] L. Labakhua, U. Nunes, R. Rodrigues, and F. S. Leite, *Smooth Trajectory Planning for Fully Automated Passengers Vehicles: Spline and Clothoid Based Methods and Its Simulation*. Springer Berlin Heidelberg, 2008, pp. 169–182.

[12] J. A. R. Silva and V. Grassi, "Path planning at roundabouts using piecewise linear continuous curvature curves," in *Proceedings Latin American Robotics Symposium (LARS) and Brazilian Symposium on Robotics (SBR)*, 2017, pp. 1–6.
[13] M. Rodrigues, A. McGordon, G. Gest, and J. Marco, "Autonomous navigation in interaction-based environments—a case of non-signalized roundabouts," *IEEE Transactions on Intelligent Vehicles*, vol. 3, no. 4, pp. 425–438, 2018.
[14] C. Hidalgo, R. Lattarulo, J. Pérez, and E. Asua, "Hybrid trajectory planning approach for roundabout merging scenarios," in *Proceedings IEEE International Conference on Connected Vehicles and Expo (ICCVE)*, 2019, pp. 1–6.
[15] R. Tian, S. Li, N. Li, I. Kolmanovsky, A. Girard, and Y. Yildiz, "Adaptive game-theoretic decision making for autonomous vehicle control at roundabouts," in *Proceedings IEEE Conference on Decision and Control (CDC)*, 2018, pp. 321–326.
[16] J. F. Medina-Lee, A. Artuñedo, J. Godoy, and J. Villagra, "Merit-based motion planning for autonomous vehicles in urban scenarios," *Sensors*, vol. 21, no. 11, pp. 1–25, 2021.
[17] S. Wen and G. Guo, "Distributed trajectory optimization and sliding mode control of heterogenous vehicular platoons," *IEEE Transactions on Intelligent Transportation Systems*, vol. 23, no. 7, pp. 7096–7111, 2022.
[18] A. Breuer, J.-A. Termöhlen, S. Homoceanu, and T. Fingscheidt, "opendd: A large-scale roundabout drone dataset," in *Proceedings IEEE International Conference on Intelligent Transportation Systems (ITSC)*, 2020, pp. 1–6.
[19] F. Poggenhans, J.-H. Pauls, J. Janosovits, S. Orf, M. Naumann, F. Kuhnt, and M. Mayr, "Lanelet2: A high-definition map framework for the future of automated driving," in *Proceedings IEEE International Conference on Intelligent Transportation Systems (ITSC)*, 2018, pp. 1672–1679.
[20] J. Godoy, V. Jiménez, A. Artuñedo, and J. Villagra, "A grid-based framework for collective perception in autonomous vehicles," *Sensors*, vol. 21, no. 3, pp. 1–21, 2021.
[21] V. Trentin, A. Artuñedo, J. Godoy, and J. Villagra, "Interaction-aware intention estimation at roundabouts," *IEEE Access*, vol. 9, no. 1, pp. 123 088–123 102, 2021.
[22] J. F. Medina-Lee, A. Artuñedo, J. Godoy, and J. Villagra, "Reachability estimation in dynamic driving scenes for autonomous vehicles," in *Proceedings IEEE Intelligent Vehicles Symposium (IV)*, 2020, pp. 2133–2139.
[23] AVSimulation, "Scaner studio 1.9," https://www.avsimulation.fr/solutions/\#studio, accessed: 2021-05-11.
[24] J. F. Medina-Lee, V. Trentin, and J. Villagra, "Framework for motion prediction of vehicles in a simulation environment," in *Proceedings Jornádas de Automática*, 2019, pp. 520–527.
[25] J. Eggert and T. Puphal, "Continuous risk measures for adas and ad," in *Proceedings Future Active Safety Technology Symposium*, 2017, pp. 1–8.

VI. Biography Section

Juan Medina-Lee graduated as an Electronic Engineer from the Universidad del Quindío, Colombia in 2012. In 2016 received his Master degree in Engineering from the Universidad del Valle. His research areas of interest are decision making, embedded systems, and robotics. He worked as a professor in the University of Quindío, teaching subjects in digital systems area and robotics from 2012 until 2018. He is currently working as a researcher in the Centre for Automation and Robotics (UPM-CSIC) as a member of AUTOPIA Program and studying a Ph.D. degree on robotics at the Universidad Politécnica de Madrid.

Jorge Godoy was born in Maracay, Venezuela, in 1986. He received the degree in electronics engineering from Universidad Simón Bolívar in 2008, and the M.E. and Ph.D. degrees in automation and robotics from the Universidad Politécnica de Madrid in 2011 and 2013, respectively. From 2013 to 2017, he was the Technical Coordinator of the AUTOPIA Program funded by research contracts from National and European research projects. His research interests include intelligent transportation systems, autonomous driving, path planning, and embedded AI-based control for autonomous vehicles. In 2009, he was granted with a Pre-Doctoral JAE Fellowship from CSIC for researching on autonomous vehicles at the Centre for Automation and Robotics (UPM-CSIC). In November 2017, he was granted with a Juan de la Cierva Fellowship for Post-Doctoral Research at the Universidad Politécnica de Madrid.

Antonio Artuñedo received the B.Sc. degree in electrical engineering from the Universidad de Castilla–La Mancha, Spain, in 2011, the M.Sc. degree in industrial engineering from the Universidad Carlos III de Madrid in 2014, and the Ph.D. degree in automation and robotics from the Technical University of Madrid (UPM), Spain, in 2019, with the AUTOPIA Program. During his Pre-Doctoral period, he made a research stay at the Integrated Vehicle Safety Group at TNO, The Netherlands, in 2017. He is currently a Post-Doctoral Researcher with the Centre for Automation and Robotics (UPM-CSIC), AUTOPIA Program, Madrid, Spain. He has been working on both national and European research projects in the scope of autonomous vehicles. He has published and peer-reviewed multiple journals and conference papers focused in this field. His research interests include system modeling and simulation, intelligent control, motion planning, and decision-making systems. His thesis won the prize to the best Ph.D. on Intelligent Transportation Systems 2020 by the Spanish Chapter of the IEEE-ITS Society.

Jorge Villagra graduated in industrial engineering from the Universidad Politécnica of Madrid in 2002. He received the Ph.D. degree in real-time computer science, robotics and automatic control from the École des Mines de Paris, France, in 2006. From 2007 to 2009, he was a Visiting Professor with the Universidad Carlos III of Madrid, Spain. From August 2013 to August 2016, he led the Department of ADAS and Highly Automated Driving Systems at Ixion Industry and Aerospace SL, where he also coordinated all the activities in the EU Research and Development funding programmes. He has been leading AUTOPIA Program at CSIC, since October 2016. He has developed his research activity in six different entities with a very intense activity in project setup and management, through over 40 international and national R&D projects, where he is or has been IP of 17 of these projects. He has published over 100 articles in international journals and in international conferences on autonomous driving, intelligent transportation systems, model-free control, and probabilistic approaches for embedded components in autonomous vehicles.